Weyl semimetals with S_4 symmetry

Yuting Qian,[1,2] Jiacheng Gao,[1,2] Zhida Song,[3] Simin Nie,[4] Zhijun Wang,[1,2,*] Hongming Weng,[1,2,5,6,†] and Zhong Fang[1,2]

[1]*Beijing National Laboratory for Condensed Matter Physics, and Institute of Physics, Chinese Academy of Sciences, Beijing 100190, China*

[2]*University of Chinese Academy of Sciences, Beijing 100049, China*

[3]*Department of Physics, Princeton University, Princeton, New Jersey 08544, USA*

[4]*Department of Materials Science and Engineering, Stanford University, Stanford, California 94305, USA*

[5]*Songshan Lake Materials Laboratory, Dongguan, Guangdong 523808, China*

[6]*CAS Center for Excellence in Topological Quantum Computation, University of Chinese Academy of Sciences, Beijing 100190, China*

(Received 19 December 2019; accepted 1 April 2020; published 28 April 2020)

In time-reversal-breaking centrosymmetric systems, the appearance of Weyl points can be guaranteed by an odd number of even/odd-parity occupied bands at eight inversion-symmetry-invariant momenta. Here, based on symmetry analysis and first-principles calculations, we demonstrate that for time-reversal-invariant systems with S_4 symmetry, the Weyl semimetal phase can be characterized by the inequality between a well-defined invariant η and an S_4 indicator z_2. By applying this criterion, we find that some candidates, previously predicted to be topological insulators, are actually Weyl semimetals in the noncentrosymmetric space group with S_4 symmetry. Our first-principles calculations show that four pairs of Weyl points are located in the $k_{x,y} = 0$ planes, with each plane containing four same-chirality Weyl points. An effective model has been built and captures the nontrivial topology in these materials. Our strategy to find the Weyl points by using symmetry indicators and invariants opens a new route to search for Weyl semimetals in time-reversal-invariant systems.

DOI: 10.1103/PhysRevB.101.155143

I. INTRODUCTION

Topological materials have attracted a lot of attention in the past few decades [1–13]. Many candidates of topological insulators (TIs) are predicted theoretically first and verified experimentally later [12–16]. Most of the predictions are indicated by topological invariants or symmetry indicators [17–24]. Topological Weyl semimetals (WSMs) [25–35] show linear dispersion around discrete doubly degenerate points, termed the Weyl points, which are regarded as the sinks/sources of Berry curvature in momentum space. They exhibit many exotic properties, such as Fermi-arc states [2,36–38] on the surfaces, chiral anomaly [39,40], anomalous Hall effect [41,42], etc. However, as Weyl points in three-dimensional (3D) momentum space do *not* require any specific symmetry protection (but the lattice translation symmetry), WSMs usually *cannot* be predicted based on topological invariants or symmetry indicators in the time-reversal-invariant (TRI) systems. As we know, for the time-reversal-breaking (TRB) centrosymmetric systems, the appearance of Weyl points can be guaranteed by an odd number of even/odd-parity occupied bands at eight inversion-symmetry-invariant (ISI) momenta [33,43,44], which can be simply understood by two unequal Chern numbers (if well-defined) of two parallel ISI planes [shown in Figs. 1(a) and 1(b)]. Here, our aim is to find proper topological invariants or symmetry indicators in the TRI systems, which warrant the WSM phase.

In this work, we focus on the TRI systems with S_4 symmetry (a more general description of S_4-invariant systems is given in Ref. [45]). For these systems, we define a topological invariant η as

$$(-1)^{\eta} = (-1)^{\nu_{a_1}} (-1)^{\nu_{a_2}},$$

which is well defined as long as there are two gapped parallel TRI planes (e.g., the a_1-plane and the a_2-plane). The invariants, ν_{a_1} and ν_{a_2}, are the time-reversal $\mathbb{Z}_2$ invariants [46] of the two parallel TRI planes, respectively. In addition, the S_4 symmetry defines a symmetry indicator z_2 [19,20]. Note that a centrosymmetric TRI system always satisfies $\eta = z_2$ if it is well defined [17,19]. Here, we find that the inequality between η and z_2 indicates the appearance of Weyl points generally (without considering additional symmetries). Explicitly, a candidate with $\eta \neq z_2$ can be a WSM, as shown in Figs. 1(b) and 1(d).

Several years ago, many compounds were predicted to be TIs in the noncentrosymmetric structure of space group 121 ($I\bar{4}2m$) [47]. However, after we have carefully investigated these so-called "TIs," we find that they can actually be classified into two different cases based on the S_4 indicator: $z_2 = 1$ (Case I) and $z_2 = 0$ (Case II). In this work, we demonstrate that the "TIs" in Case II virtually turn out to be WSMs. Four pairs of Weyl points are found in the $k_{x,y} = 0$ planes, with each plane containing four same-chirality Weyl points. Moreover, the Weyl points are located exactly at the charge-neutrality level. The WSM phase is characterized by the inequality between η and z_2 (i.e., $\eta \neq z_2$), which is also applicable to the WSMs in other space groups with S_4 symmetry [48,49]. To capture the nontrivial topology of the materials in space group 121, we have constructed a six-band low-energy effective

*wzj@iphy.ac.cn
†hmweng@iphy.ac.cn

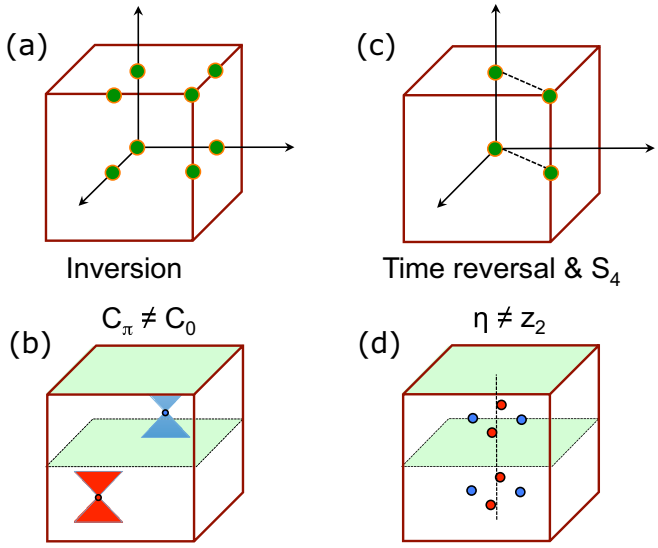

FIG. 1. Schematic WSMs with symmetry indicators and topological invariants. For a TRB centrosymmetric system, an odd number of even/odd-parity occupied bands at eight ISI momenta [green dots in (a)] reveals that the Chern numbers of the two ISI planes are different, which guarantees the appearance of odd pairs of Weyl points in the 3D Brillouin zone (BZ) (b). Note that there is always an even number of even/odd-parity occupied bands in a TRI system. For a TRI and S_4-symmetric system, a z_2 indicator is defined on four S_4 invariant momenta [green dots in (c)], and the inequality between the invariant η (defined in the main text) and S_4 z_2 indicator reveals the appearance of Weyl points, as shown in (d). The red (blue) dots stand for $+1$ (-1) chiral Weyl points.

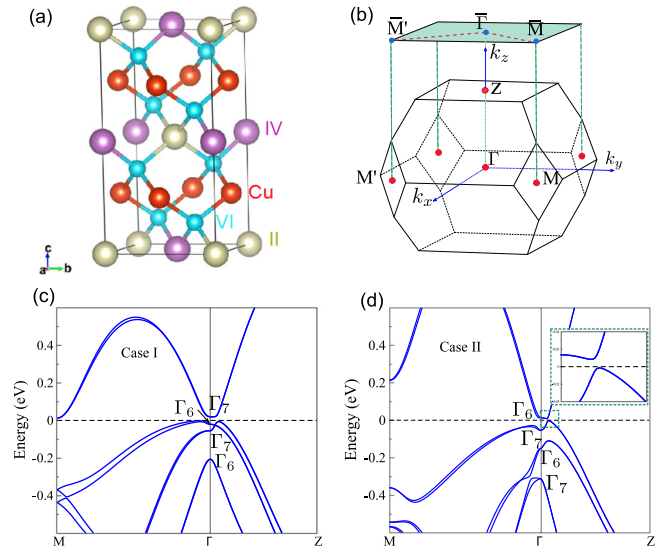

FIG. 2. (a) Crystal structure of the quaternary stannite Cu_2-II-IV-VI_4 compounds and (b) BZ for the series of compounds in space group 121. There are alternating cation layers of mixed II and IV atoms, which are separated from each other by layers of Cu monovalent cations. Two equivalent Cu atoms, one II atom, one IV atom and four VI atoms occupy the $4d$, $2a$, $2b$, and $8i$ Wyckoff positions, respectively. In the Cu_2-Cu-Sb-VI_4 structure, the $2a$ and $2b$ positions are occupied by Cu and Sb atoms, respectively. The electronic band structures and irreps at the Γ point with SOC for (c) Cu_3SbS_4 and (d) $Cu_2ZnGeSe_4$ are presented for Case I and Case II, respectively.

model. Fermi arcs as iconic surface states of the WSM have also been presented. Our strategy to find the Weyl points by using symmetry indicators and invariants opens a new route to search for Weyl semimetals in the TRI systems.

II. CRYSTAL STRUCTURE AND METHODOLOGY

We investigated a series of Cu-based chalcogenides in the stannite structure: Cu_2-Cu-Sb-VI_4 and Cu_2-II-IV-VI_4 with II={Cd, Hg, and Zn}, IV={Si, Ge, and Sn}, and VI={S, Se, and Te}. The series of compounds in space group $I\bar{4}2m$ (D_{2d}) have a body-centered-tetragonal crystal structure with lattice parameters: a and c. The structure has three twofold rotational symmetries ($C_{2x,2y,2z}$), two mirror symmetries ($M_{xy,\bar{x}y}$), and the combined S_4 symmetry of inversion symmetry (I) and the fourfold rotation (C_{4z}). But, neither I nor C_{4z} is respected. Figure 2(a) presents the stannite structure. Each anion is tetrahedrally coordinated by four cations with three inequivalent bonds: VI-Cu, VI-II, and VI-IV. The crystal structure is nearly double zinc-blende structure along the c axis but with a little distortion characterized by $c \neq 2a$, due to the interlayer coupling. These compounds represent the strained HgTe-class materials [49].

We performed the first-principles calculations with the VASP package [50,51] based on the density functional theory (DFT) with the projector augmented wave (PAW) method [52,53]. The generalized gradient approximation (GGA) with exchange-correlation functional of Perdew, Burke, and Ernzerhof (PBE) for the exchange-correlation functional [54] was employed. The kinetic energy cutoff was set to 400 eV for the plane-wave basis. A $10 \times 10 \times 10$ k-mesh in the self-consistent process for the BZ sampling was adopted. The lattice and atomic parameters in the Inorganic Crystal Structure Database (ICSD) were employed in our calculations, as shown in Table II in Appendix A. The electronic structures with spin-orbit coupling (SOC) were carried out. The Wilson-loop technique [55] was used to calculate topological invariants and chiral charges [42].

III. RESULTS AND DISCUSSIONS

A. Electronic band structures

Based on first-principles calculations, we have reinvestigated the electronic band structures of the compounds, which are proposed to be TIs in the previous work of Ref. [47]. We find that these compounds can actually be classified into two cases. In the main text, we take Cu_3SbS_4 (Case I) and $Cu_2ZnGeSe_4$ (Case II) compounds as two examples of the two cases, respectively, and we present the results of the other candidates in the Appendix A. The calculated band structures along high-symmetry lines are presented in Fig. 2. One can find that there is a band gap along the high-symmetry lines for both compounds. Then, we have calculated the time-reversal $\mathbb{Z}_2$ invariants in both $k_z = 0$ and $k_z = \frac{\pi}{c}$ planes. The results of the Wilson loop calculations are presented in Fig. 6 of Appendix A. The two $\mathbb{Z}_2$ invariants are computed to be $\nu_{k_z=0} = 1$ and $\nu_{k_z=\frac{\pi}{c}} = 0$, giving rise to $\eta = 1$ (or $\nu_0 = 1$ if the

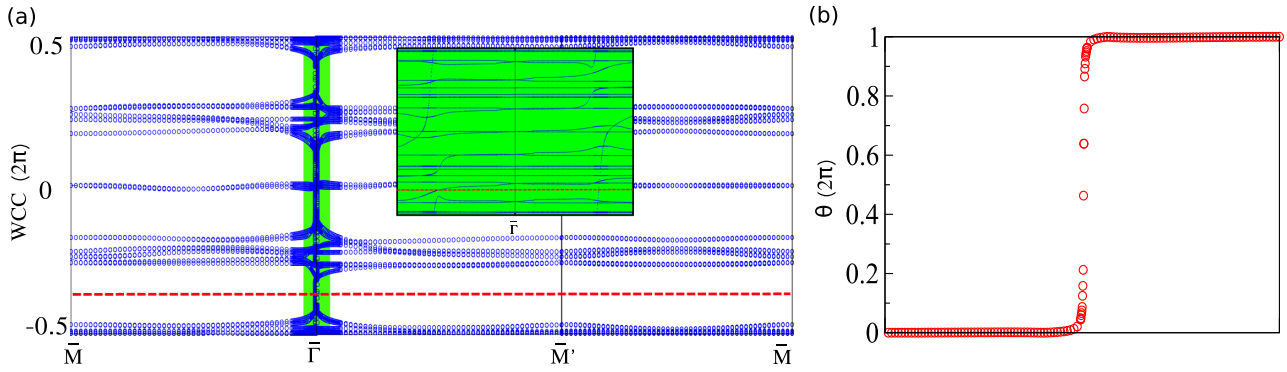

FIG. 3. (a) The WCC of k_z-directed Wilson loops of $Cu_2ZnGeSe_4$ on the path $\bar{M}(0.5, 0.5) - \bar{\Gamma}(0, 0) - \bar{M}'(0.5, -0.5) - \bar{M}(0.5, 0.5)$ as marked in Fig. 2. (b) The chirality of the Weyl point at $[0.0036(\frac{2\pi}{a}), 0.0, 0.0657(\frac{2\pi}{c})]$ calculated by the Wilson-loop method on a manifold enclosing it.

system is fully gapped in the 3D BZ [17]). These results seem to be consistent with the previous prediction of "TIs" [47]. In this paper, the "TIs" refer to these topological compounds previously predicted in space group 121, which host $\eta = 1$.

We have further checked irreducible representations (irreps) of electronic states [56]. In Case I, the Γ_7 band is the lowest conduction band (LCB) at Γ, while the LCB is the Γ_6 band in Case II. The Γ_6 and Γ_7 irreps are labeled by the little group of Γ (the double group of D_{2d}). In a body-centered structure, four S_{4z} invariant momenta (SIM) are $\Gamma[0, 0, 0]$, $C[0, 0, 1]$, $A[0.5, 0.5, 0.5]$, and $B[0.5, 0.5, -0.5]$ (hereafter, all k points are given in units of $[\frac{2\pi}{a}, \frac{2\pi}{a}, \frac{2\pi}{c}]$ in Cartesian coordinates). Note that the A and B points are not TRI k-points. Since $S_4^4 = -1$ in a spinful system, the eigenvalues of S_4 symmetry are given as $\lambda_j = e^{i\pi\frac{2j-1}{4}}$ with $j \in \{0, 1, 2, 3\}$. The z_2 indicator of S_4 symmetry in a body-centered structure is defined explicitly as follows:

$$z_2 = \sum_{K\in\{\Gamma,C,A,B\}} \frac{n_K^2 - n_K^0}{2} \mod 2,$$

with n_K^i the number of occupied bands with S_4 eigenvalue λ_i at the SIM K, which is slightly different from the definition in Ref. [20] (see more details in Appendix C and Ref. [45]). The z_2 indicator is computed to be 1 and 0 for Case I and Case II (see Table III in Appendix C), respectively.

In the 3D insulating phase, the strong TI (STI) index ν_0 [17] is defined on eight distinct TRI momenta $[\Gamma_{i=(n_1n_2n_3)} = (n_1\mathbf{b}_1 + n_2\mathbf{b}_2 + n_3\mathbf{b}_3)/2$ with $n_j = 0, 1$ and $\mathbf{b}_j$ primitive reciprocal-lattice vectors]:

$$(-1)^{\nu_0} = \prod_{n_j=0,1} \delta_{n_1n_2n_3} = (-1)^{\nu_{a_1}}(-1)^{\nu_{a_2}},$$

where $\delta_i = \sqrt{\det[w(\Gamma_i)]}/\mathrm{Pf}[w(\Gamma_i)]$ with the unitary matrix $w_{ij}(\mathbf{k}) = \langle u_i(\mathbf{k})|\mathcal{T}|u_j(\mathbf{k})\rangle$. Here $|u_j(\mathbf{k})\rangle$ is the periodic part of the Bloch wave function. At $\mathbf{k} = \Gamma_i$, $w_{ij} = -w_{ji}$, so the Pfaffian $\mathrm{Pf}[w(\Gamma_i)]$ is well-defined. Since the product of four δ_i defines the $\mathbb{Z}_2$ invariant of the 2D TRI plane (if the four Γ_i form a plane), the STI indicator ν_0 can also be defined by two distinct $\mathbb{Z}_2$ invariants (ν_{a_1} and ν_{a_2}) in the two parallel TRI planes (the a_1-plane and the a_2-plane) [57], which yields $\eta = \nu_0$ for an insulator. Note that ν_0 is well defined if the 3D bulk states are fully gapped while η is well-defined as long as there are two fully gapped TRI planes. On the other hand, in the presence of an additional symmetry S_4, the z_2 indicator of S_4 symmetry is presented to be identical to the STI indicator ν_0 for the insulators [19,20]. Therefore, the "TIs" in Case II in space group 121 with a trivial z_2 indicator *cannot* be insulators. Consequently, we find that those candidates are virtually WSMs, with four pairs of Weyl points being at the charge-neutrality level.

B. Weyl points and Wilson loop calculations

To locate the positions of the Weyl points, we have calculated the k_z-directed Wilson loops of the WSM $Cu_2ZnGeSe_4$ along the following path: $\bar{M}[0.5, 0.5] - \bar{\Gamma}[0, 0] - \bar{M}'[0.5, -0.5] - \bar{M}[0.5, 0.5]$ (in units of $[\frac{2\pi}{a}, \frac{2\pi}{a}]$) in the k_xk_y plane. The results in Fig. 3(a) show that it has a nontrivial Chern number $C = +2$, which implies that at least two Weyl points with charge $+1$ are enclosed in the 2D manifold spanned by the in-plane path and the k_z axis [42]. First, let us assume there is a Weyl point with charge $+1$ at a general point $[x_1(\frac{2\pi}{a}), y_1(\frac{2\pi}{a}), z_1(\frac{2\pi}{c})]$ in the manifold. Since it is fully gapped in the $k_z = 0$ plane, z_1 should be nonzero (i.e., $z_1 \neq 0$). Then, the combined symmetry $\mathcal{T}C_{2z}$ shows that there is also a Weyl point at $[x_1, y_1, -z_1]$ with the

TABLE I. The fitting parameters of the six-band model for the Cu_3SbS_4 (Case I) and $Cu_2ZnGeSe_4$ (Case II) compounds.

Phases	A_0 (eV)	A_1 (eV Å^2)	A_2 (eV Å^2)	B_0 (eV)	B_1 (eV Å^2)	B_2 (eV Å^2)	C_1 (eV Å^2)	C_2 (eV Å^2)	C_3 (eV Å)	δ_1 (eV Å)	δ_2 (eV Å)	δ_3 (eV Å^3)
TI	−0.055	25.121	28.679	−0.001	−6.642	−2.872	0.244	4.691	0.325	0.020	0.013	1.103
WSM	−0.151	27.895	18.702	−0.020	−5.451	−2.369	0.300	3.300	1.137	−0.034	1.300	4.400

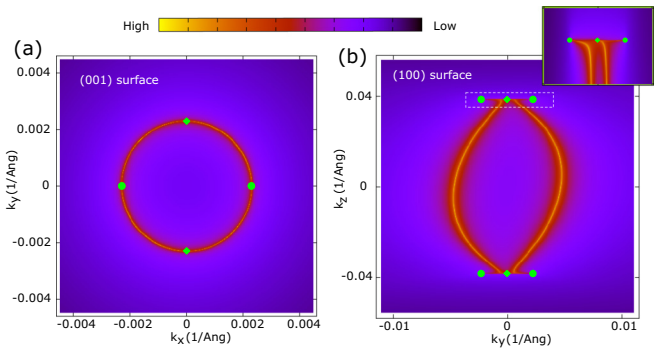

FIG. 4. Surface Fermi arcs of the six-band model. (a) Surface Fermi arcs in the (001) surface BZ. (b) Surface Fermi arcs in the (100) surface BZ. The projected Weyl points are shown as square and circle points for different chiralities.

same chiral charge +1. Lastly, if the Weyl points are away from the $k_y = 0$ plane, the number of Weyl points enclosed in the manifold must be a multiple of 4 with the same topological chiral charge due to the two antiunitary symmetries: $\mathcal{T}C_{2y}$ and $\mathcal{T}C_{2z}$. Thus, the corresponding Chern number along the path has to be a multiple of 4. However, this is obviously not the case in this compound. Therefore, we conjecture that the Weyl points are located in the $k_y = 0$ plane: $(x_1, 0, \pm z_1)$. After carefully checking the energy gap and topological chiral charge in half of the $k_y = 0$ plane (i.e., $k_x > 0$), we do find two Weyl points at $[0.0036, 0.0, \pm 0.0657]$. The topological chiral charge is computed with the Wilson-loop method on an enclosed manifold surrounding the Weyl point. The results of the Weyl point [0.0036,0.0,0.0657] are shown in Fig. 3(b) and its topological charge is read to be +1. Considering the two Weyl points with the same chiral charge, it is consistent with the total Chern number ($C = +2$) in Fig. 3(a).

C. Effective model and Fermi arcs

To capture the nontrivial topology of these compounds, we build a six-band effective model, which includes four valence bands (Γ_6 and Γ_7) and two conduction bands (Γ_6). Under the basis of $\{|xyz\uparrow\rangle, i|xyz\downarrow\rangle, |\frac{3}{2}, \frac{3}{2}\rangle, |\frac{3}{2}, \frac{1}{2}\rangle, |\frac{3}{2}, -\frac{1}{2}\rangle, |\frac{3}{2}, -\frac{3}{2}\rangle\}$, the D_{2d}-invariant $\boldsymbol{k}\cdot\boldsymbol{p}$ Hamiltonian can be given as follows:

$$H(\mathbf{k}) = \begin{bmatrix} M_0 & C_3\mathbb{S}^\dagger \\ C_3\mathbb{S} & H_0 + \delta_1 H_A + \delta_2 H_B + \delta_3 H_C \end{bmatrix},$$

where $M_0 = (A_0 + A_1 k_z^2 + A_2 k_{||}^2)\mathbb{I}_2$ and $H_0 = (B_0 + B_1 k_z^2 + B_2 k_{||}^2)\mathbb{I}_4 + C_1\mathbb{E} + C_2\mathbb{T}$ ($\mathbb{I}_n$ is the $n \times n$ identity matrix, and see the explicit matrices of $\mathbb{E}$, $\mathbb{T}$, $\mathbb{S}$, and H_C in Appendix D), $H_A = \mathrm{diag}\{1, -1, -1, 1\}$, and

$$H_B = \begin{pmatrix} 0 & -k_+ & 2k_z & -\sqrt{3}k_- \\ -k_- & 0 & \sqrt{3}k_+ & -2k_z \\ 2k_z & \sqrt{3}k_- & 0 & -k_+ \\ -\sqrt{3}k_+ & -2k_z & -k_- & 0 \end{pmatrix}.$$

When $A_1 = A_2$, $B_1 = B_2$, $\delta_1 = \delta_2 = \delta_3 = 0$, it is actually O_h-invariant. The H_A term is a uniaxial strain, which reduces the symmetry to D_{4h}. The H_B term is critical, which breaks both I and C_{4z} but keeps S_{4z}. The $A_{1,2} > 0$ and $B_{1,2} < 0$ stand for the four valence bands and two conduction bands in the origin ($A_0 > B_0$). The $A_0 < B_0$ represents the band inversion happening at Γ. As a result, the $k_z = 0$ plane has a nontrivial $\mathbb{Z}_2$ invariant with four occupied bands (i.e., $\nu_{k_z=0} = 1$). If $\delta_1 > 0$, it is a TI without gapless points. If $\delta_1 < 0$, it is a WSM with four pairs of Weyl points. The fitting parameters for Cu_3SbS_4 and $Cu_2ZnGeSe_4$ are given in Table I and the corresponding band structures can be found in Fig. 5.

To obtain the Fermi-arc states [2,41] of the WSM in Case II, we transform the six-band model into a tight-binding model on a tetragonal lattice by introducing the following substitutions: $k_i \to \frac{1}{L_i}\sin[k_i L_i]$ and $k_i^2 \to \frac{2}{L_i^2}(1 - \cos[k_i L_i])$ with $i = x, y, z$ [4]. We use an iterative method to obtain the surface Green's function of the semi-infinite system [58,59]. The imaginary part of the surface Green's function is the local density of states (LDOS) at the surface. The obtained LDOSs on semi-infinite (001) and (100) surfaces are presented in Fig. 4. Since the Weyl points are exactly located at the charge-neutrality level, we only see the Fermi-arc states connecting the projections of the Weyl points. On the (001) surface, two same-chirality Weyl points project onto the same projection, so each projection has two arc states. On the (100) surface, the projected topological charges are presented in Fig. 4(b). Two arc states have to go across the $k_z = 0$ line, because it is the edge of the $k_z = 0$ plane with a nontrivial $\mathbb{Z}_2$ invariant.

IV. DISCUSSION

To check the stability of the band inversion in these WSMs (see Table II in Appendix A) in space group 121, we have performed more accurate calculations by using a modified Becke-Johnson (mBJ) potential. The evolutions of the energy levels of the four bands at Γ (three valence bands and one conduction band) are presented in Appendix B as a function of the mBJ parameter (C_{mBJ}). The results show that the band inversion features for $Cu_2HgGeTe_4$, Cu_3SbSe_4, $Cu_2HgSnSe_4$, and $Cu_2HgSnTe_4$ are relatively more reliable. Among them, $Cu_2HgSnTe_4$ is the most promising candidate in the WSM

TABLE II. ICSD numbers and topological classifications for these topological compounds with SOC.

Compound	ICSD Num.	Previous work	This work	Compound	ICSD Num.	Previous work	This work [units: ($\frac{2\pi}{a}$, $\frac{2\pi}{a}$, $\frac{2\pi}{c}$)]
Cu_3SbS_4	628824 [63]	TI [47]	TI	$Cu_2ZnGeSe_4$	627831 [64]	TI [47]	WSM (0.0036, 0.0, 0.0657)
$Cu_2HgSiTe_4$	656152 [65]	TI [11,21]	TI	$Cu_2ZnSnSe_4$	629099 [66]	TI [47]	WSM (0.0037, 0.0, 0.0757)
$Cu_2HgGeSe_4$	627692 [66]	TI [47]	TI	$Cu_2CdSnSe_4$	619784 [66]	TI [47]	WSM (0.0014, 0.0, 0.0294)
$Cu_2HgGeTe_4$	656155 [65]	TI [11,21]	TI	$Cu_2HgSnSe_4$	627936 [66]	TI [47]	WSM (0.0049, 0.0, 0.0238)
Cu_3SbSe_4	628997 [63]	TI [11,21]	TI	$Cu_2HgSnTe_4$	627940 [66]	Trivial [11,21]	WSM (0.0082, 0.0, 0.0338)

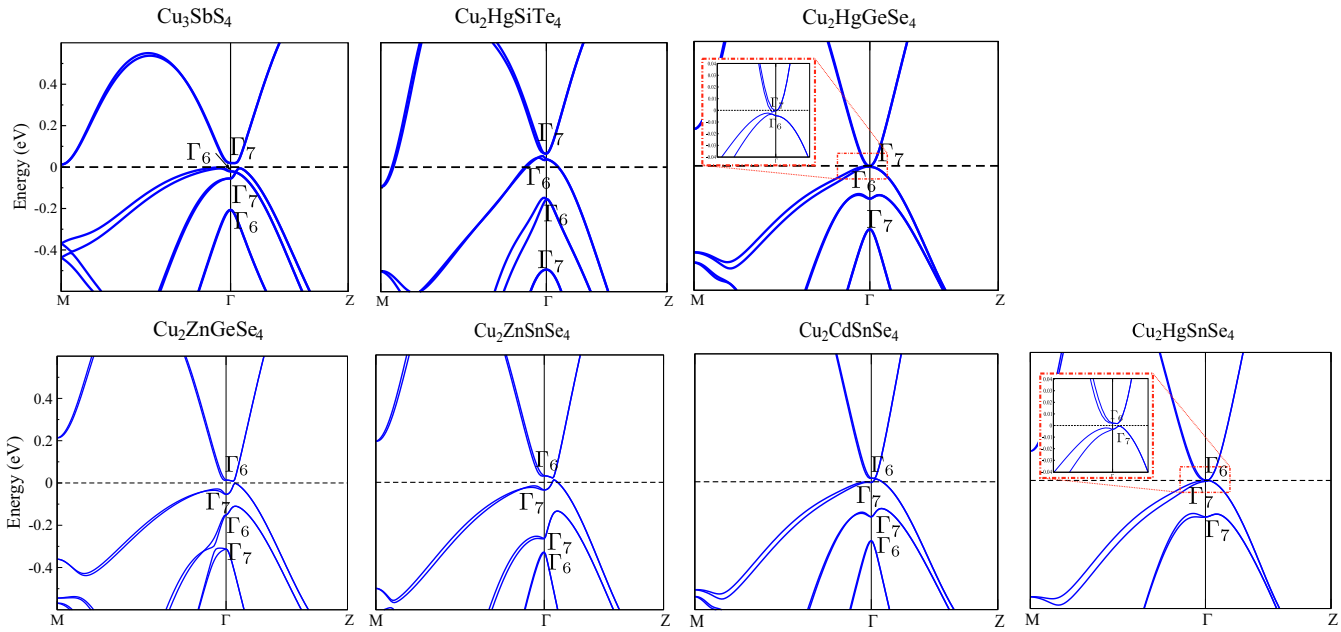

FIG. 5. The electronic energy bands with SOC and band irreps at the Γ point of topological compounds with $\eta = 1$. Explicitly, these compounds have a nontrivial $\mathbb{Z}_2$ invariant in the $k_z = 0$ plane, but a trivial $\mathbb{Z}_2$ invariant in the $k_z = \frac{\pi}{c}$ plane.

phase, with the band inversion happening at a relatively large $C_{\mathrm{mBJ}} = 1.25$. In the very recent experiment [60], the semimetallic feature of $Cu_2HgSnSe_4$ has been observed in STM and ARPES data.

The criterion of $\eta \neq z_2$ for a WSM phase can be widely applied to other space groups with S_4 symmetry. For example, we have computed the indicator z_2 and the invariant η of the WSM $CuTlSe_2$ of space group 122 [48], which was also previously predicted to be a TI [61]. The obtained results of $\eta = 1$ and $z_2 = 0$ are consistent with the WSM phase. In addition, this criterion can be used to understand the robustness of the WSM phase (compressive strain) and the TI phase (tensile strain) of the strained HgTe material as well [49].

In summary, based on the DFT calculations, we demonstrate that the previously predicted "TIs" in space group 121, which have S_{4z} symmetry but no inversion symmetry, can be actually classified into two cases: $z_2 = 1$ (Case I) and $z_2 = 0$ (Case II). The common characteristic of these "TIs" is that the time-reversal $\mathbb{Z}_2$ invariants are 1 and 0 for the $k_z = 0$ and $k_z = \frac{\pi}{c}$ planes, respectively, resulting in $\eta = 1$. It is consistent with $S_4\, z_2 = 1$ in Case I for an insulating phase. But, the "TIs" with $S_4\, z_2 = 0$ in Case II are actually WSMs, which were not revealed before. They are also serving as typical examples of topological materials with *trivial* symmetry indicators [20,62]. Four pairs of Weyl points are found in the $k_{x,y} = 0$ planes, with each plane having four Weyl points with the same topological chiral charge. Our work corrects the topological knowledge of these compounds and predicts more WSM candidates, which can be further checked in experiments. More importantly, the strategy to find the Weyl points in the TRI systems with symmetry indicators and invariants (i.e., $\eta \neq z_2$) opens a new route to search for WSMs [45], which could largely stimulate the prediction of the WSMs.

ACKNOWLEDGMENTS

We thank Prof. H.-J. Zhang for helpful discussions. This work was supported by the National Natural Science Foundation of China (Grants No. 11974395, No. 11504117, No. 11674369, No. 11925408) and the Chinese Academy of Sciences (Grant No. XDB33000000). H.W. acknowledges support from the National Key Research and Development Program of China (Grants No. 2016YFA0300600, No. 2016YFA0302400, and No. 2018YFA0305700), the K. C. Wong Education Foundation (Grant No. GJTD-2018-01). Z.W. acknowledges support from the National

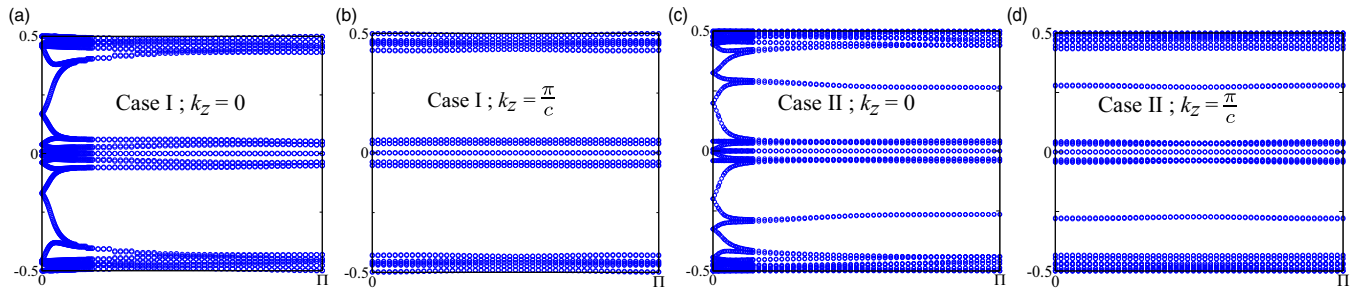

FIG. 6. The calculated time-reversal $\mathbb{Z}_2$ in $k_z = 0$ and $k_z = \frac{\pi}{c}$ planes for Case I (a,b) and Case II (c,d), respectively.

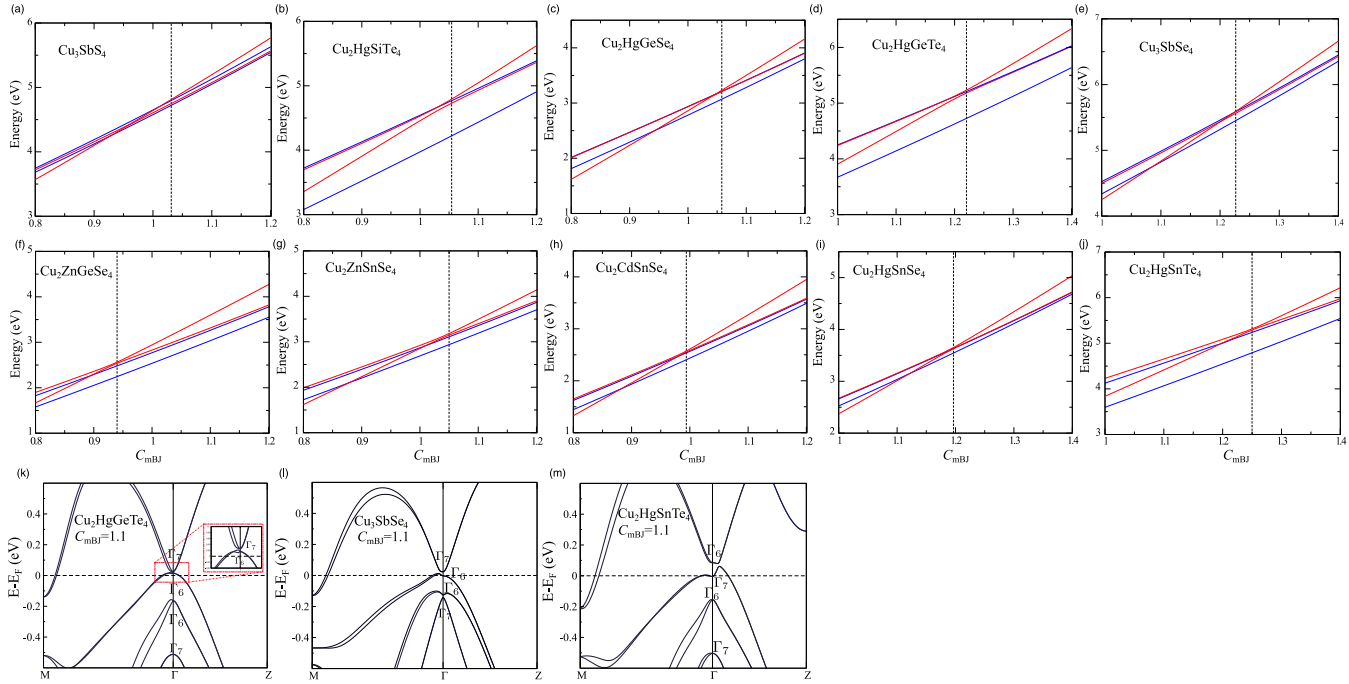

FIG. 7. Parts (a)–(j) show the band evolutions of four bands near the Fermi level (three valence bands and one conduction band) at the Γ point with varying the parameter C_{mBJ} for different topological compounds. The Γ_6 and Γ_7 bands are denoted by the red and blue lines, respectively. Parts (k)–(m) present the SOC electronic structures with $C_{\mathrm{mBJ}} = 1.1$ for $Cu_2HgGeTe_4$ (k), Cu_3SbSe_4 (l), and $Cu_2HgSnTe_4$ (m), respectively.

Thousand-Young-Talents Program and the CAS Pioneer Hundred Talents Program.

Y. Q. and J. G. contributed equally to this work.

APPENDIX A: TOPOLOGICAL MATERIALS WITH $\eta = 1$

For the series of compounds in space group 121, we have systematically computed band structures and time-reversal $\mathbb{Z}_2$ invariants in the two planes $k_z = 0$ and $k_z = \frac{\pi}{c}$ as shown in Figs. 5 and 6, respectively. The experimental parameters are employed as reported in the ICSD (shown in Table II). We present the band structures of the topological compounds with $\eta = 1$. For all these topological compounds, $\nu_{k_z=0} = 1$ and $\nu_{k_z=\frac{\pi}{c}} = 0$ are in the two planes, respectively. These topological compounds were previously predicted to be TIs [47]. However, after we determine the irreps of the low-energy bands [56], one can easily find that they can actually be classified into two cases: Case I has the Γ_7 band as the LCB (the upper panels of Fig. 5), while Case II has the Γ_6 band as the LCB (the lower panels of Fig. 5). In the following discussion, we show that the two cases actually correspond to different values of the S_4 z_2 indicator.

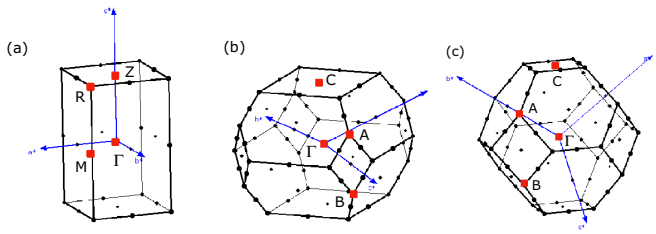

FIG. 8. The 3D BZs and SIM points. We present the 3D BZs for simple lattice (a), body-centered lattice (b), and face-centered lattice (c), respectively. The SIM points are labeled, too.

APPENDIX B: THE ACCURATE CALCULATIONS WITH THE MBJ MODIFICATIONS

Because the band gap is usually underestimated by the PBE functional, we have performed the more accurate calculations by using a modified Beche-Johnson (mBJ) potential. Since the key feature of these band structures is the energy ordering at Γ, we have systematically presented the evolutions of the energy bands at Γ as a function of the mBJ parameter (C_{mBJ}) for different compounds in Fig. 7. We found that the relative energies of the valence bands almost do not change with varying C_{mBJ}. The energy ordering of Case I is Γ_7, Γ_6, and Γ_7 (from higher energy to lower energy), while it is Γ_6, Γ_7, and Γ_7 for Case II. Upon decreasing the parameter C_{mBJ}, one can clearly see that the energy of the Γ_6 conduction band decreases monotonically. Accordingly, the Γ_6 conduction band "intersects" with those three valence bands (guided by eye, in principle, two Γ_6 bands cannot meet each other at Γ). In Fig. 7, the critical C_{mBJ} is denoted by the dashed lines, indicating the band inversion between the Γ_6 conduction band and the highest valence band.

TABLE III. The number of occupied states with S_4 eigenvalue λ_2 and λ_0 at SIM. The last column shows the determined S_4 z_2 indicator.

n_K^2, n_K^0	Γ	C	A	B	S_4 z_2
Case I (TI)	15,16	16,15	16,15	16,15	1
Case II (WSM)	14,17	16,15	15,16	15,16	0

TABLE IV. The matrix representations of the generators (i.e., $C_{3,111}$ and C_{4z}) of O_h, given under the basis of Γ_7^- and Γ_8^+, respectively.

	Γ_7^-	Γ_8^+
$C_{3,111}$	$\frac{1}{2}\begin{pmatrix} 1-i & -1-i \\ 1-i & 1+i \end{pmatrix}$	$\frac{1}{4}\begin{pmatrix} -1-i & -\sqrt{3}+\sqrt{3}i & \sqrt{3}+\sqrt{3}i & 1-i \\ -\sqrt{3}-\sqrt{3}i & -1+i & -1-i & -\sqrt{3}+\sqrt{3}i \\ -\sqrt{3}-\sqrt{3}i & 1-i & -1-i & \sqrt{3}-\sqrt{3}i \\ -1-i & \sqrt{3}-\sqrt{3}i & \sqrt{3}+\sqrt{3}i & -1+i \end{pmatrix}$
C_{4z}	$-\frac{\sqrt{2}}{2}\begin{pmatrix} 1-i & 0 \\ 0 & 1+i \end{pmatrix}$	$\begin{pmatrix} -(-1)^{\frac{1}{4}} & 0 & 0 & 0 \\ 0 & -(-1)^{\frac{3}{4}} & 0 & 0 \\ 0 & 0 & (-1)^{\frac{1}{4}} & 0 \\ 0 & 0 & 0 & (-1)^{\frac{3}{4}} \end{pmatrix}$
I	$-\mathbb{I}_2$	$\mathbb{I}_4$
$\mathcal{T}$	$-\begin{pmatrix} 0 & -1 \\ 1 & 0 \end{pmatrix}K$	$\begin{pmatrix} 0 & 0 & 0 & 1 \\ 0 & 0 & -1 & 0 \\ 0 & 1 & 0 & 0 \\ -1 & 0 & 0 & 0 \end{pmatrix}K$

The results show that the critical C_{mBJ} parameters for $Cu_2HgGeTe_4$, Cu_3SbSe_4, $Cu_2HgSnSe_4$, and $Cu_2HgSnTe_4$ are relatively large, about 1.2, which indicates that the band inversion is more reliable in these compounds.

APPENDIX C: $S_4 z_2$ INDICATOR IN THESE TOPOLOGICAL COMPOUNDS

Since $S_4^4 = -1$ in a spinful system, the eigenvalues of S_4 symmetry are given as $\lambda_j = e^{i\pi\frac{2j-1}{4}}$ with $j \in \{0, 1, 2, 3\}$. In the TRI systems with S_4 symmetry, we propose a generalized definition of the z_2 indicator of S_4 symmetry:

$$z_2 = \sum_{K\in\{\text{four SIM}\}} \frac{n_K^2 - n_K^0}{2} \mod 2, \tag{C1}$$

with n_K^i the number of occupied bands with S_4 eigenvalue λ_i at the SIM K. The detailed derivation is presented in Ref. [45]. It is identical to the definition in Refs. [19,20] if all four SIM are also time-reversal invariant momenta (TRIM) (see Fig. 8).

In a simple tetragonal structure (SG 81 and its father space groups), the four SIM are $\Gamma[0, 0, 0]$, $Z[0, 0, 0.5]$, $M[0.5, 0.5, 0.0]$, and $R[0.5, 0.5, 0.5]$ (the k points are given in units of $[\frac{2\pi}{a}, \frac{2\pi}{a}, \frac{2\pi}{c}]$ in Cartesian coordinates). Since the four SIM are also TRIM, all the bands are doubly degenerate. Thus, $n_K^{\frac{1}{2}}$ ($n_K^{\frac{3}{2}}$) is equal to n_K^0 (n_K^2). As defined in Refs. [19,20], $n_K^{\frac{1}{2}}$ ($n_K^{\frac{3}{2}}$) is the number of Kramers pairs at K with $\mathrm{tr}[D(S_4)] = \sqrt{2}$ (with $\mathrm{tr}[D(S_4)] = -\sqrt{2}$), and $D(S_4)$ is the representation matrix on the corresponding Kramers pair,

$$z_2 = \sum_{K\in\{\Gamma,Z,M,R\}} \frac{n_K^{\frac{3}{2}} - n_K^{\frac{1}{2}}}{2} \mod 2, \tag{C2}$$

In a body-centered-tetragonal structure (SG 82 and its father space groups), four SIM are $\Gamma[0, 0, 0]$, $C[0, 0, 1]$, $A[0.5, 0.5, 0.5]$, and $B[0.5, 0.5, -0.5]$ (the k points are given in units of $[\frac{2\pi}{a}, \frac{2\pi}{a}, \frac{2\pi}{c}]$ in Cartesian coordinates). Note that the A and B points are not TRIM. Namely, there is no Kramers pair at A and B. So, the S_4 z_2 indicator is redefined as

$$z_2 = \sum_{K\in\{\Gamma,C,A,B\}} \frac{n_K^2 - n_K^0}{2} \mod 2. \tag{C3}$$

Since space group 121 has a body-centered-tetragonal structure, n_K^0 and n_K^2 are computed for four SIM and listed explicitly in Table III [56]. The z_2 indicator is computed to be 1 and 0 for Case I and Case II, respectively.

In a face-centered cubic structure (SG 216 and its father space groups), four SIM are $\Gamma[0, 0, 0]$, $C[0, 0, 1]$, $A[1, 0, 0.5]$, and $B[1, 0, -0.5]$ (the k points are given in units of $[\frac{2\pi}{a}, \frac{2\pi}{a}, \frac{2\pi}{a}]$ in Cartesian coordinates). Note that A and B points are not TRIM. Namely, there is no Kramers pair at A and B. So, the S_4 z_2 indicator is redefined as

$$z_2 = \sum_{K\in\{\Gamma,C,A,B\}} \frac{n_K^2 - n_K^0}{2} \mod 2. \tag{C4}$$

APPENDIX D: SIX-BAND MODEL

Using the Γ_7^- and Γ_8^+ bands under the symmetry of O_h, one can construct a six-band effective model. Explicitly, under the basis of $\{i|xyz\uparrow\rangle, i|xyz\downarrow\rangle, |\frac{3}{2}, \frac{3}{2}\rangle, |\frac{3}{2}, \frac{1}{2}\rangle, |\frac{3}{2}, -\frac{1}{2}\rangle, |\frac{3}{2}, -\frac{3}{2}\rangle\}$, the O_h-invariant $\boldsymbol{k}\cdot\boldsymbol{p}$ Hamiltonian can be given as follows:

$$H' = \begin{bmatrix} (A_0 + A_2k^2)\mathbb{I}_2 & C_3\mathbb{S}^\dagger \\ C_3\mathbb{S} & H_0 \end{bmatrix} \tag{D1}$$

with $H_0 = (B_0 + B_2k^2)\mathbb{I}_4 + C_1\mathbb{E} + C_2\mathbb{T}$, where $k \equiv k_x^2 + k_y^2 + k_z^2$ and $\mathbb{I}_n$ is an $n-$dimensional identity matrix

$$\mathbb{E} = \begin{pmatrix} 2k_z^2 - k_x^2 - k_y^2 & 0 & \sqrt{3}(k_x^2 - k_y^2) & 0 \\ 0 & -(2k_z^2 - k_x^2 - k_y^2) & 0 & \sqrt{3}(k_x^2 - k_y^2) \\ \sqrt{3}(k_x^2 - k_y^2) & 0 & -(2k_z^2 - k_x^2 - k_y^2) & 0 \\ 0 & \sqrt{3}(k_x^2 - k_y^2) & 0 & 2k_z^2 - k_x^2 - k_y^2 \end{pmatrix}, \tag{D2}$$

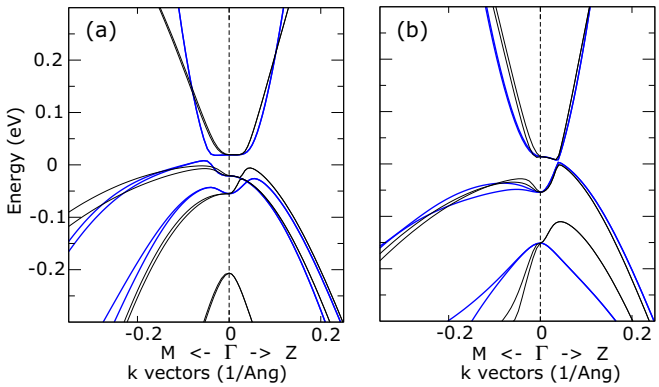

FIG. 9. The fitted electronic energy bands around the Γ point of Cu_3SbS_4 (a) and $Cu_2ZnGeSe_4$ (b) with fitting parameters shown in Table I, where the black lines are the band structures from first-principles calculations and the blue lines are the results of the fitted effective six-band model.

$$\mathbb{T} = \begin{pmatrix} 0 & k_- k_z & -ik_x k_y & 0 \\ k_+ k_z & 0 & 0 & -ik_x k_y \\ ik_x k_y & 0 & 0 & -k_- k_z \\ 0 & ik_x k_y & -k_+ k_z & 0 \end{pmatrix}, \tag{D3}$$

$$\mathbb{S} = \begin{pmatrix} k_+ & 2k_z \\ 0 & -\sqrt{3}k_+ \\ \sqrt{3}k_- & 0 \\ 2k_z & -k_- \end{pmatrix}. \tag{D4}$$

Also, the matrix representations of the generators of O_h are given in Table IV.

To obtain the D_{4h} symmetry, one can easily change A_2k^2 (B_2k^2) to $A_1k_z^2 + A_2k_{||}^2$ ($B_1k_z^2 + B_2k_{||}^2$) and add another diagonal term H_A to H_0, which is a uniaxial strain in the z-axis. Simply, H_A can take the form of Diag$\{1, -1, -1, 1\}$. Then, in order to break I and C_{4z} but keep S_{4z}, H_B (first-order of $\mathbf{k}$) and H_C (third-order of $\mathbf{k}$) are added. The D_{2d}-invariant Hamiltonian is derived as

$$H(\mathbf{k}) = \begin{bmatrix} M_0 & C_3\mathbb{S}^\dagger \\ C_3\mathbb{S} & H_0 + \delta_1 H_A + \delta_2 H_B + \delta_3 H_C \end{bmatrix},$$

where $M_0 = (A_0 + A_1k_z^2 + A_2k_{||}^2)\mathbb{I}_2$ and $H_0 = (B_0 + B_1k_z^2 + B_2k_{||}^2)\mathbb{I}_4 + C_1\mathbb{E} + C_2\mathbb{T}$ and the additional first-order term H_B,

$$H_B = \begin{pmatrix} 0 & -k_+ & 2k_z & -\sqrt{3}k_- \\ -k_- & 0 & \sqrt{3}k_+ & -2k_z \\ 2k_z & \sqrt{3}k_- & 0 & -k_+ \\ -\sqrt{3}k_+ & -2k_z & -k_- & 0 \end{pmatrix} \tag{D5}$$

and the third-order term H_C,

$$H_C = k_z(k_x^2 - k_y^2)J_z + k_x(k_y^2 - k_z^2)J_x + k_y(k_z^2 - k_x^2)J_y \tag{D6}$$

with

$$J_x = \begin{pmatrix} 0 & \sqrt{3} & 0 & 0 \\ \sqrt{3} & 0 & 2 & 0 \\ 0 & 2 & 0 & \sqrt{3} \\ 0 & 0 & \sqrt{3} & 0 \end{pmatrix},$$

$$J_y = \begin{pmatrix} 0 & -\sqrt{3}i & 0 & 0 \\ \sqrt{3}i & 0 & -2i & 0 \\ 0 & 2i & 0 & -\sqrt{3}i \\ 0 & 0 & \sqrt{3}i & 0 \end{pmatrix},$$

$$J_z = \begin{pmatrix} 3 & 0 & 0 & 0 \\ 0 & 1 & 0 & 0 \\ 0 & 0 & -1 & 0 \\ 0 & 0 & 0 & -3 \end{pmatrix}. \tag{D7}$$

With the parameters given in the main text, the band structures of the model are obtained in Fig. 9.

[1] N. P. Armitage, E. J. Mele, and A. Vishwanath, Rev. Mod. Phys. **90**, 015001 (2018).
[2] X. Wan, A. M. Turner, A. Vishwanath, and S. Y. Savrasov, Phys. Rev. B **83**, 205101 (2011).
[3] H. Weng, X. Dai, and Z. Fang, J. Phys.: Condens. Matter **28**, 303001 (2016).
[4] Z. Wang, H. Weng, Q. Wu, X. Dai, and Z. Fang, Phys. Rev. B **88**, 125427 (2013).
[5] X. L. Qi and S.-C. Zhang, Phys. Today **63**(1), 33 (2010).
[6] M. Z. Hasan and C. L. Kane, Rev. Mod. Phys. **82**, 3045 (2010).
[7] J. Cano, B. Bradlyn, Z. Wang, M. Hirschberger, N. P. Ong, and B. A. Bernevig, Phys. Rev. B **95**, 161306(R) (2017).
[8] Z. Wang, A. Alexandradinata, R. J. Cava, and B. A. Bernevig, Nature (London) **532**, 189 (2016).
[9] J. Cano, B. Bradlyn, Z. Wang, L. Elcoro, M. G. Vergniory, C. Felser, M. I. Aroyo, and B. A. Bernevig, Phys. Rev. B **97**, 035139 (2018).
[10] M. G. Vergniory, L. Elcoro, Z. Wang, J. Cano, C. Felser, M. I. Aroyo, B. A. Bernevig, and B. Bradlyn, Phys. Rev. E **96**, 023310 (2017).
[11] B. Bradlyn, L. Elcoro, J. Cano, M. G. Vergniory, Z. Wang, C. Felser, M. I. Aroyo, and B. A. Bernevig, Nature (London) **547**, 298 (2017).
[12] B. A. Bernevig, T. L. Hughes, and S.-C. Zhang, Science **314**, 1757 (2006).
[13] H. Zhang, C.-X. Liu, X.-L. Qi, X. Dai, Z. Fang, and S.-C. Zhang, Nat. Phys. **5**, 438 (2009).
[14] M. König, S. Wiedmann, C. Brüne, A. Roth, H. Buhmann, L. W. Molenkamp, X.-L. Qi, and S.-C. Zhang, Science **318**, 766 (2007).
[15] Y. Chen, J. G. Analytis, J.-H. Chu, Z. Liu, S.-K. Mo, X.-L. Qi, H. Zhang, D. Lu, X. Dai, Z. Fang *et al.*, Science **325**, 178 (2009).
[16] J. Ma, C. Yi, B. Lv, Z. Wang, S. Nie, L. Wang, L. Kong, Y. Huang, P. Richard, P. Zhang *et al.*, Sci. Adv. **3**, e1602415 (2017).
[17] L. Fu, C. L. Kane, and E. J. Mele, Phys. Rev. Lett. **98**, 106803 (2007).
[18] L. Fu and C. L. Kane, Phys. Rev. B **76**, 045302 (2007).
[19] E. Khalaf, H. C. Po, A. Vishwanath, and H. Watanabe, Phys. Rev. X **8**, 031070 (2018).

[20] Z. Song, T. Zhang, Z. Fang, and C. Fang, Nat. Commun. **9**, 3530 (2018).

[21] M. G. Vergniory, L. Elcoro, C. Felser, N. Regnault, B. A. Bernevig, and Z. Wang, Nature (London) **566**, 480 (2019).

[22] T. Zhang, Y. Jiang, Z. Song, H. Huang, Y. He, Z. Fang, H. Weng, and C. Fang, Nature (London) **566**, 475 (2019).

[23] F. Tang, H. C. Po, A. Vishwanath, and X. Wan, Nature (London) **566**, 486 (2019).

[24] J. Kruthoff, J. de Boer, J. van Wezel, C. L. Kane, and R.-J. Slager, Phys. Rev. X **7**, 041069 (2017).

[25] S. Murakami, New J. Phys. **9**, 356 (2007).

[26] J. Liu and D. Vanderbilt, Phys. Rev. B **90**, 155316 (2014).

[27] H. Weng, C. Fang, Z. Fang, B. A. Bernevig, and X. Dai, Phys. Rev. X **5**, 011029 (2015).

[28] A. A. Soluyanov, D. Gresch, Z. Wang, Q. Wu, M. Troyer, X. Dai, and B. A. Bernevig, Nature (London) **527**, 495 (2015).

[29] H. Weng, C. Fang, Z. Fang, and X. Dai, Phys. Rev. B **94**, 165201 (2016).

[30] B. Q. Lv, N. Xu, H. M. Weng, J. Z. Ma, P. Richard, X. C. Huang, L. X. Zhao, G. F. Chen, C. E. Matt, and F. Bisti, Nat. Phys. **11**, 724 (2015).

[31] B. Q. Lv, H. M. Weng, B. B. Fu, X. P. Wang, H. Miao, J. Ma, P. Richard, X. C. Huang, L. X. Zhao, G. F. Chen, Z. Fang, X. Dai, T. Qian, and H. Ding, Phys. Rev. X **5**, 031013 (2015).

[32] S. Nie, G. Xu, F. B. Prinz, and S.-C. Zhang, Proc. Natl. Acad. Sci. (USA) **114**, 10596 (2017).

[33] Z. Wang, M. G. Vergniory, S. Kushwaha, M. Hirschberger, E. V. Chulkov, A. Ernst, N. P. Ong, R. J. Cava, and B. A. Bernevig, Phys. Rev. Lett. **117**, 236401 (2016).

[34] V. Ivanov and S. Y. Savrasov, Phys. Rev. B **99**, 125124 (2019).

[35] A. Sakai, Y. P. Mizuta, A. A. Nugroho, R. Sihombing, T. Koretsune, M. T. Suzuki, N. Takemori, R. Ishii, D. Nishio-Hamane, R. Arita *et al.*, Nat. Phys. **14**, 1119 (2018).

[36] N. Xu, H. Weng, B. Lv, C. E. Matt, J. Park, F. Bisti, V. N. Strocov, D. Gawryluk, E. Pomjakushina, K. Conder *et al.*, Nat. Commun. **7**, 11006 (2016).

[37] S.-Y. Xu, I. Belopolski, N. Alidoust, M. Neupane, G. Bian, C. Zhang, R. Sankar, G. Chang, Z. Yuan, C.-C. Lee *et al.*, Science **349**, 613 (2015).

[38] C. Wang, Y. Zhang, J. Huang, S. Nie, G. Liu, A. Liang, Y. Zhang, B. Shen, J. Liu, C. Hu *et al.*, Phys. Rev. B **94**, 241119(R) (2016).

[39] X. Huang, L. Zhao, Y. Long, P. Wang, D. Chen, Z. Yang, H. Liang, M. Xue, H. Weng, Z. Fang *et al.*, Phys. Rev. X **5**, 031023 (2015).

[40] C.-L. Zhang, S.-Y. Xu, I. Belopolski, Z. Yuan, Z. Lin, B. Tong, G. Bian, N. Alidoust, C.-C. Lee, S.-M. Huang *et al.*, Nat. Commun. **7**, 10735 (2016).

[41] G. Xu, H. Weng, Z. Wang, X. Dai, and Z. Fang, Phys. Rev. Lett **107**, 186806 (2011).

[42] Z. Fang, N. Nagaosa, K. S. Takahashi, A. Asamitsu, R. Mathieu, T. Ogasawara, H. Yamada, M. Kawasaki, Y. Tokura, and K. Terakura, Science **302**, 92 (2003).

[43] T. L. Hughes, E. Prodan, and B. A. Bernevig, Phys. Rev. B **83**, 245132 (2010).

[44] S. Nie, Y. Sun, F. B. Prinz, Z. Wang, H. Weng, Z. Fang, and X. Dai, Phys. Rev. Lett. **124**, 076403 (2020).

[45] J. Gao, Y. Qian, S. Nie, Z. Wang, H. Weng, and Z. Fang, arXiv:2004.09489.

[46] C. L. Kane and E. J. Mele, Phys. Rev. Lett. **95**, 146802 (2005).

[47] Y. J. Wang, H. Lin, T. Das, M. Z. Hasan, and A. Bansil, New J. Phys. **13**, 085017 (2010).

[48] J. Ruan, S.-K. Jian, D. Zhang, H. Yao, H. Zhang, S.-C. Zhang, and D. Xing, Phys. Rev. Lett. **116**, 226801 (2016).

[49] J. Ruan, S.-K. Jian, H. Yan, H. Zhang, S.-C. Zhang, and D. Xing, Nat. Commun. **7**, 11136 (2016).

[50] G. Kresse and J. Furthmüller, Comput. Mater. Sci. **6**, 15 (1996).

[51] G. Kresse and J. Furthmüller, Phys. Rev. B **54**, 11169 (1996).

[52] P. E. Blöchl, Phys. Rev. B **50**, 17953 (1994).

[53] G. Kresse and D. Joubert, Phys. Rev. B **59**, 1758 (1999).

[54] J. P. Perdew, K. Burke, and M. Ernzerhof, Phys. Rev. Lett. **77**, 3865 (1996).

[55] R. Yu, X. L. Qi, A. Bernevig, Z. Fang, and X. Dai, Phys. Rev. B **84**, 075119 (2011).

[56] J. Gao, Q. Wu, C. Persson, and Z. Wang, arXiv:2002.04032.

[57] D. Gresch, G. Autès, O. V. Yazyev, M. Troyer, D. Vanderbilt, B. A. Bernevig, and A. A. Soluyanov, Phys. Rev. B **95**, 075146 (2017).

[58] Q. Wu, S. Zhang, H.-F. Song, M. Troyer, and A. A. Soluyanov, Comput. Phys. Commun. **224**, 405 (2018).

[59] M. P. L. Sancho, J. M. L. Sancho, J. M. L. Sancho, and J. Rubio, J. Phys. F **15**, 851 (1985).

[60] Y.-Y. Lv, L. Cao, Q.-Q. Yuan, S.-S. Chen, Z.-Q. Shi, Q.-Y. Li, Y. B. Chen, S.-H. Yao, J. Zhou, H. Wang *et al.*, Phys. Rev. B **100**, 195147 (2019).

[61] W. Feng, D. Xiao, J. Ding, and Y. Yao, Phys. Rev. Lett. **106**, 016402 (2011).

[62] Z. Wang, B. J. Wieder, J. Li, B. Yan, and B. A. Bernevig, Phys. Rev. Lett. **123**, 186401 (2019).

[63] R. Annamamedov, L. Berger, V. Petrov, and S. Slobodchikov, Inorg. Mater. **3**, 1195 (1967).

[64] L. Guen, W. Glaunsinger, and A. Wold, Mater. Res. Bull. **14**, 463 (1979).

[65] H. Haeuseler, F. W. Ohrendorf, and M. Himmrich, Z. Naturforsch., B **46**, 1049 (1991).

[66] H. Hahn and H. Schulz, Naturwissenschaften **52**, 426 (1965).